Sediment phosphorus composition controls hot spots and hot moments of internal loading in a temperate reservoir

Ellen A. Albright[1] and Grace M. Wilkinson[1]

[1]Center for Limnology, University of Wisconsin-Madison, 680 N. Park St., Madison, WI 53706

Corresponding author: Ellen A. Albright (ealbright2@wisc.edu)

ABSTRACT

Phosphorus (P) flux across the sediment-water interface in lakes and reservoirs responds to external perturbations within the context of sediment characteristics. Lentic ecosystems experience profound spatiotemporal heterogeneity in the mechanisms that control sediment P fluxes, likely producing hot spots and hot moments of internal loading. However, spatiotemporal variation in P fluxes remains poorly quantified, particularly in the context of sediment chemistry as a controlling variable. We measured P flux rates and mobile sediment P forms along the longitudinal gradient of a temperate reservoir every two months from February to October of 2020. Both aerobic and anaerobic processes mobilized sediment P throughout the year. High flux rates at littoral sampling sites (8.4 and 9.7 mg P m^{-2} day^{-1}) occurred in late summer under oxic conditions and mobilized labile organic P. High fluxes at the profundal site coincided with hypolimnetic anoxia under ice cover and in mid-summer (11.2 and 17.2 mg P m^{-2} day^{-1}, respectively) and released redox-sensitive P. Several high fluxes substantially skewed the flux rate distribution, providing evidence of hot spots and hot moments of internal loading. We further analyzed the ecosystem-level effects of elevated sediment P release by scaling measured flux rates to representative areas of the lakebed and estimating P loads. We found that aerobic P release from littoral sites had an outsized impact on total loads. Our findings demonstrate that focusing solely on flux rates without ecosystem context can lead to misidentification of the dominant biogeochemical mechanisms involved and ultimately impede eutrophication management.

Key words

Phosphorus; Sediments; Spatial Variability; Seasonality; Dissolved Oxygen; Reservoir

Highlights

- Evidence of hot spots and hot moments of sediment P fluxes in a temperate reservoir
- Sediment P release occurs across a broad range of dissolved oxygen concentrations
- Sediment P composition controls flux response to dissolved oxygen availability

INTRODUCTION

An ecosystem's response to external perturbations results from the interaction of fast- and slow-acting state variables, which fall along a gradient of turnover times from short to long, respectively (Carpenter and Turner 2000). Slow variables determine ecosystem context and control how fast variables respond to external drivers (Walker and others 2012). Understanding how slow and fast variables interact is necessary for the study and management of complex systems (Crépin 2007, Ward and others 2019). For example, eutrophication in lakes and reservoirs is often influenced by interacting slow and fast variables at the sediment-water interface. Sediments hold a pool of phosphorus (P), which is the legacy of past external loading and subsequent sedimentation (Søndergaard and others 2003, Walsh and others 2019). This P may be retained in the sediments or mobilized and released into the overlying water (i.e., internal P loading; Orihel and others 2017). Within the sediments there are many different P-containing minerals, organic compounds, and surface complexes, which are vulnerable to different mechanisms of internal loading (North and other 2015, Orihel and others 2017). As such, the chemical composition of the sediment P pool is a pivotal slow variable that shapes how the rate of P flux from the sediments (i.e., the fast variable) responds to fluctuations in external drivers (Carpenter 2003).

The response of sediment P flux rates to changing dissolved oxygen availability, the result of external drivers, is shaped by the forms of P present in the sediment. For example, if redox-sensitive P forms (i.e., those associated with iron or manganese oxides) dominate the sediment P pool, then hypolimnetic oxygen depletion will trigger P release due to reductive dissolution of the host minerals (Mortimer 1941, Jensen and Andersen 1992). When a mixing event or other external disturbance delivers dissolved oxygen to the sediment surface, oxidized iron and manganese minerals will stabilize P, resulting in sediment P retention. The idea that oxic conditions prevent P release and that internal loading primarily occurs under anoxia is a persistent paradigm in limnology. However, there is ample evidence that internal P loading occurs under a range of dissolved oxygen conditions based on sediment characteristics (Hupfer and Lewandowski 2008). If sediments hold a large pool of labile organic P, then oxic conditions are expected to mobilize and release P via microbial decomposition and mineralization (Joshi and others 2015, Horppila and others 2017). In this case, an influx of dissolved oxygen to the lakebed would stimulate rather than suppress internal loading through this mechanism. The relationship between dissolved oxygen and P flux is expected to vary with the composition of the sediment P pool, which is heterogenous across the lakebed and over time (Nowlin and others 2005, Kowalczewska-Madura and others 2019). However, it is unclear how the interaction between this slow variable and external drivers influences spatiotemporal variability in sediment P fluxes and what the consequences of this variation are at the ecosystem scale.

Lentic ecosystems are highly variable in space and time. Temperate reservoirs are particularly variable due to longitudinal gradients in basin morphometry as well as strong spatial and seasonal variation in thermal mixing, hypolimnetic dissolved oxygen, and organic matter sedimentation (Nowlin and others 2005, Hayes and others 2017, Cardoso-Silva and others 2018). Increasing water depth from riverine to lacustrine regions of a reservoir yields spatial variation in water column mixing and thus chemical conditions at the sediment-water interface (Kimmel and Groeger 1984, Hudson and Vandergucht 2015). Specifically, shallow riverine and transitional sections remain mixed throughout the open water season, usually maintaining oxygenated conditions above the sediments. Conversely, the deeper lacustrine region will likely experience at least intermittent thermal stratification, which may result in hypolimnetic dissolved oxygen depletion (Hayes and others 2017). In short, basin morphometry produces spatial variation in the dynamics of external drivers that influence internal P loading. Organic matter sedimentation also varies along the longitudinal gradient and may impact the composition of the sediment P pool. Riverine segments receive more allochthonous organic matter inputs while autochthonous material dominates sedimentation in the lacustrine region (Hayes and others 2017, Cardoso-Silva and others 2018). Autochthonous organic matter inputs also vary over space and time due to seasonal algal dynamics and spatial heterogeneity in bloom formation (Buelo and others 2018, Ortiz and Wilkinson 2021). When combined, spatial and seasonal variation in both redox conditions and the composition of the sediment P pool likely produce hot spots and hot moments of sediment P flux.

Hot spots and hot moments are high rates of biogeochemical activity that occur when two reactants are brought together in space and time within an ecosystem (McClain and others 2003). This biogeochemical phenomenon can be understood within the conceptual framework of fast and slow variables. Specifically, a hot spot-hot moment is the product of an external perturbation delivering a reactant that interacts with the slow variable resulting in a high rate in the fast variable at that moment and location. For example, sudden water column mixing due to a storm delivers dissolved oxygen to the sediment surface, which is rich in labile organic P, resulting in a spike of sediment P release due to aerobic decomposition and mineralization (Tammeorg and others 2016). This external perturbation interacts with the slow variable (i.e., the sediment P pool) and brings two reactants together (i.e., dissolved oxygen and labile organic P), resulting in the hot spot-hot moment. Hot spots and hot moments disproportionately influence elemental cycles at the ecosystem-scale. Although the importance of hot spots and hot moments has been well-documented, analyses of the underlying mechanisms remain scarce (McClain and others 2003). Additionally, most studies have focused on carbon and nitrogen cycles in streams and riparian soils, and there has been little consideration of hot spots and hot moments of P cycling, especially in lentic ecosystems (Bernhardt and others 2017). Even though temperate waterbodies likely experience hot spots and hot moments of internal P loading, no study to date has explicitly quantified these extreme events and identified the causal mechanisms.

In order to quantify hot spots and hot moments of sediment P flux and explore the underlying mechanisms, we measured mobile sediment P pools and fluxes over the course of a year and across the lakebed of a temperate reservoir (Figure 1). Specifically, we measured sediment P composition and flux rates at three sites along the longitudinal gradient of the reservoir approximately every other month over the course of 2020, capturing conditions under the ice as well as thermal mixing and stratification events during the open water season. We asked, (Q1) When and where do hot spots and hot moments of sediment P flux rates occur, and what are the underlying mechanisms? (Q2) How does the slow variable (i.e., the composition of the sediment P pool) change over space and time, and how do these changes relate to P flux rates? (Q3) How do hot spots and hot moments of internal loading scale to the ecosystem level? We hypothesize that there are hot spots and hot moments in the rates of P flux from the sediments that arise from interactions between P speciation and biogeochemical conditions at the sediment-water interface. Over the course of the year, we anticipate that P will be mobilized and released from a variety of sediment P sources. We anticipate that temperature and dissolved oxygen concentrations will be key mechanisms driving internal loading but that the specific effects of these variables will depend on the composition of the sediment P pool. Predicting the occurrence of hot spots and hot moments of internal loading and identifying the causal mechanisms is essential for effectively managing whole-lake P cycling. Our analysis provides novel insights on spatiotemporal variation in lentic P cycling and the underlying mechanisms driving sediment P fluxes.

METHODS

Study Site

Green Valley Lake (GVL) is a hypereutrophic reservoir located in southwest Iowa, USA (41°05'58.9"N 94°23'04.7"W, Figure 1), with a discontinuous cold polymictic stratification and mixing pattern. The reservoir lies in the rolling loess prairie region of the western corn belt plains. Row crop agriculture dominates the GVL watershed with 68.4% of the land cover in a corn-soybean rotation. GVL is relatively small (surface area 156.2 ha) and shallow (maximum depth 6.8 m and mean depth 3.2 m), with two main branches meeting at the southern end of the basin above the dam outflow. As an impoundment of several small tributaries, GVL has a highly irregular shape (shoreline development factor 3.44), characterized by numerous shallow bays and an extensive littoral zone.

We measured spatial variation in sediment P pools and fluxes at three sampling sites distributed along the longitudinal gradient of the west branch of the reservoir. We selected the western branch as this inflow is the main tributary to the reservoir and drains the majority of the watershed. The shallow sampling site (2.5 m) was located near the west inlet, and the water column remained mixed throughout the open water season. The intermediate depth site (4.0 m) was in the middle of the western branch of GVL. Thermal stratification developed under ice and intermittently throughout the open water season. The deep sampling site (maximum water depth 6.8 m) was located at the deepest hole of the reservoir near the dam. Water column stratification and mixing followed the same pattern as the intermediate site (Table 1).

In order to evaluate seasonal patterns in P dynamics, we sampled these sites throughout 2020 on day of year (DOY) 39, 117, 181, 223, and 298 (winter, spring, mid-summer, late summer, and autumn, respectively). The timing of the sampling events was designed to capture ice cover, thermal stratification in spring, and mixing events in the summer and autumn (Table 1). The shallow site was not sampled in February due to unsafe ice conditions created by a congregation of Canada geese (*Branta canadensis*). The sampling event in late summer occurred immediately following a derecho, an intense windstorm affecting a large geographic area (Corfidi and others 2016, Goff and others 2021). Although GVL lay at the edge of the derecho’s path, windspeeds at the reservoir are estimated to have exceeded 65 kph, fully mixing the water column at all sites (Table 1).

Vertical Profiles and Water Chemistry

To monitor thermal mixing patterns in GVL, we deployed vertical strings of temperature sensors at the shallow and deep sites (HOBO 8K Pendant Temperature Data Logger). Sensors were placed every 0.5 m up to 3 m deep and then every 1 m to the lakebed. The sensors logged water temperature every 30 minutes from spring to late summer. At each sampling site and event, we also measured water column profiles of temperature and dissolved oxygen using a YSI ProDSS Multiparameter Digital Water Quality Meter. Additionally, we collected water samples 0.25 m below the water surface and 0.5 m above the sediment-water interface for analysis of total P (TP), soluble reactive P (SRP), total nitrogen, nitrate, and suspended solids (see Supplementary Material for full methods and data). Subsamples were filtered in the lab (0.45µm GF/C filters) for SRP analysis, and all samples were preserved with concentrated sulfuric acid to pH 2. TP samples underwent persulfate digestion prior to analysis (Standard Methods 4500-P B.5). We measured SRP and TP concentrations with the molybdenum blue method modified from Murphy and Riley (1962; Standard Methods 4500-P E) using a SEAL Analytical AQ2 Discrete Analyzer.

Sediment P Fluxes

To quantify sediment P fluxes, we collected intact sediment cores and incubated them under ambient conditions in the lab while measuring P exchange with the overlying water. For each sampling site and event, three replicate sediment cores were collected using a gravity corer (inner diameter 5 cm, length 50 cm), such that there were approximately 25 cm of sediment and

25 cm of overlying water. The sediment cores and the overlying water were sealed in clear, acrylic core sleeves and transported at 4°C. In the laboratory, we exposed cores to temperature and dissolved oxygen treatments corresponding to ambient conditions at each site. Temperature treatments were achieved by securing the cores in either a water bath or an incubation chamber. Dissolved oxygen levels were manipulated by bubbling either air mixtures or N_2 through the overlying water. A slow, consistent bubble rate was used to gently mix the water column without disturbing the sediment surface. After the cores were placed in the incubation system, we measured the height of the water column within each core tube to calculate the water volume.

Samples of the overlying water were collected 12, 36, 60, and 84 hours after the initial incubation set-up. For each daily sampling, 50 mL of water was removed for analysis of TP. An equivalent volume of hypolimnetic water, collected from 0.5 m above the sediment surface at the corresponding site, was used to replace the volume removed. The replacement hypolimnetic water was also analyzed for TP daily to account for changes in water column P due to sampling and water replacement. Samples were preserved with concentrated sulfuric acid to pH 2 and stored at 4°C before undergoing persulfate digestion and analysis for TP (Standard Methods 4500-P B.5, E). We monitored water temperature, dissolved oxygen, and pH (YSI ProDSS Multiparameter Digital Water Quality Meter) daily to ensure that the overlying water remained representative of ambient conditions in the reservoir at the time of sampling.

The change in TP in the overlying water was used to calculate daily, areal P flux rates for each core. We first calculated the mass of P in the overlying water immediately following the collection of the daily water sample as well as the mass of P in the replacement water. We then determined how the addition of the replacement water changed the TP concentration of the overlying water. The daily change in TP concentration was calculated as the difference between this new TP concentration after the addition of replacement water and the TP concentration measured in the water column the next day (see Supplementary Material for equations). The P flux rate was then calculated as:

$$\text{P flux rate (mg P m}^{-2}\text{ day}^{-1}) = (C_t - C_0) * V / A / d \qquad \text{(Eq. 1)}$$

Where C_t is the water column TP concentration on a given day, C_0 is the TP concentration from the previous day after the addition of replacement water, V is the total volume of water overlying the sediment core, A is the area of the sediment surface, and d is the number of days between measurements (Ogdahl and others 2014). Over a 4-day incubation, we calculated three daily P flux rates for each sediment core. We took the mean of these temporal replicates to yield one P flux rate per core, per incubation. Mean flux rate and standard error of the mean for the three replicate sediment cores from each sampling site and event were then used to estimate P flux rate through time at the various sites.

Sediment P Content and Composition

At each sampling site and event, we collected an additional sediment core for analysis of sediment P composition, total P content, and physical characteristics (see Supplementary Material for sediment physical characteristics methods). We extruded the first 10 cm of the sediment profile into an acrylic core sleeve, which was sealed immediately to maintain ambient redox conditions. The top 10 cm of sediment is considered actively exchanging with the overlying water as diffusive processes can occur in sediments this deep (Boström & Pettersson 1982, Forsberg 1989). Samples were transported and stored at 4°C until analysis, which began within 18 to 36 hours of sample collection. Sediments were handled under N_2-atmosphere in a glove bag and thoroughly homogenized before removing three replicate subsamples from each core. The replicates were analyzed for four mobile P species (loosely-bound, redox-sensitive, aluminum-bound, and labile organic P) via sequential extraction following Lukkari and others (2007). Dried sediments were used to quantify total P.

To begin the sequential P extractions, subsamples of fresh sediment equivalent to 0.5 g of dry sediment were weighed into polyethylene centrifuge tubes. This same sediment pellet was used throughout the sequential extraction procedure. All extractions were performed on an orbital shaker table at 25°C. Extractant and rinse solution volumes (50 mL), shaker table speed (200 rpm), and centrifuge time and speed (30 minutes at 3000 rpm) were consistent across all extractions. In general, each extraction involved shaking the sediment pellet in the extraction solution, centrifuging, and pouring off the supernatant. All extractions included at least one rinse, in which the sediment pellet would shake for 15 minutes in a rinse solution to minimize tailing. The supernatant of the rinse extractions was combined with the primary extraction supernatant. Following each extraction, the total supernatant was preserved with concentrated sulfuric acid to pH 2 to keep metals soluble and achieve the required pH for color development during SRP and TP analyses. All SRP and TP concentrations were corrected for the extractant volume and the mass of sediment used to determine the P concentration per gram of dry sediment (See Supplementary Material for all equations).

Loosely-sorbed and pore water P were extracted in 0.46 M N_2-purged sodium chloride (NaCl) for one hour. One rinse in 0.46 M N_2-purged NaCl was used, and the combined extract solution was preserved for TP analysis (Standard Methods 4500-P B.5, E). Redox-sensitive P species were extracted in a 0.11 M bicarbonate – 0.1 M sodium dithionate (BD) solution for one hour. This extraction included two rinses with BD solution and one NaCl rinse. The combined extract supernatant was bubbled with compressed air for at least 90 minutes to remove dithionite before being preserved for TP analysis. Labile organic P and P associated with aluminum oxides were determined with an 18-hour extraction in 0.1 M sodium hydroxide (NaOH). One NaOH rinse was used, followed by one NaCl rinse. The combined extract supernatant was analyzed in two portions. First, a portion was filtered (0.45µm GF/C filters) and analyzed for SRP (Standard Methods 4500-P E). This SRP concentration was used to calculate the sediment concentration of aluminum-bound P. The remaining supernatant was digested and analyzed for TP. The labile organic P fraction was determined as the difference between the total NaOH-extractable P and the aluminum-bound P. Total sediment P concentrations were measured following a hot acid digestion on dried, ground, and homogenized sediments. Three replicate subsamples (0.2 g) of the dried sediment were combusted it at 550°C for 2 hours and then boiled on a digestion block in 50 mL of 1 M HCl for 2 hours at 150°C. Following digestion, samples were diluted to 50 mL with deionized water, and adjusted to pH 2 using 0.1 M NaOH before TP analysis.

Statistical Analyses

As there is no universal, quantitative method for delineating hot spots and hot moments of biogeochemical fluxes in a distribution of flux measurements (Bernhardt and others 2017), we used a variety of approaches to explore the distribution of P flux rates and determine whether the observed spatiotemporal variation indicated hot spots or hot moments. We first identified statistical outliers in the distribution, defined as flux measurements falling above or below 1.5 times the interquartile range. We further quantified the shape of the P flux distribution by calculating skewness (m_3; see Supplementary Material for equation), which identifies whether the distribution is symmetric ($m_3 < 0.5$) or if extreme flux rates, presumably due to hot spots or moments, skew the distribution ($m_3 > 0.5$). We further evaluated the influence of high flux rates on the distribution by iteratively removing the highest flux rates and recalculating skewness. Through this process, we determined how many of the highest flux rates would need to be removed to produce a nearly symmetric distribution (Gakuruh 2017).

In order to evaluate how the composition of the sediment P pool varied across sites and seasons, we performed a compositional data analysis. Compositional data analysis tests for a difference of proportions among multivariate observations, allowing us to test differences in the relative abundance of P fractions across different sites and events (Filzmoser and others 2018). The compositional analysis was defined by the concentrations of loosely-bound (porewater and surface sorbed), redox-sensitive (Fe- and Mn-bound), aluminum-bound, and labile organic P. The sediment P concentrations were center logratio transformed prior to a principal components analysis (PCA) on the covariance matrix, as not to bias the analysis to the most abundant sediment P fractions.

To estimate the total sediment P load (kg day^{-1}) in the reservoir for each sampling event, we multiplied the mean P flux rate (mg m^{-2} day^{-1}) at each sampling site by the lakebed area (m^{-2}) within representative depth contours corresponding to each site. The shallow site measurements were assigned to the 1.2 – 3.6 m depth contour, the intermediate depth site measurements were assigned the 3.6 – 5.6 m depth contour, and the deep site measurements were assigned the 5.6 – 6.8 m depth contour. The threshold of 5.6 m was determined based on the historical mean depth of hypoxia in the water column. We excluded areas shallower than 1.2 m, including the sediment retention basins north of the reservoir, because these areas are mainly in secluded, wind-protected bays (Figure 1). Our sampling sites, which were centrally located along a branch of the reservoir, cannot reasonably be extrapolated to these shallow areas due to expected differences in wave disturbance and the depositional environment (Kleeberg and others 2013). To calculate the lakebed area within the representative depth contours, we used the length of each depth contour from a bathymetric map produced by the Iowa Department of Natural Resources. The area between depth contours is a trapezoid-shaped area of lakebed wrapping around the reservoir basin. We calculated this area as:

$$A = \left(\frac{length\ 1 + length\ 2}{2}\right) \times h \quad \text{(Eq. 2)}$$

Where length 1 and 2 are the lengths of the bounding depth contours, and h is the assumed average distance between the depth contours across the lakebed, estimated using the Pythagorean theorem:

$$h = \sqrt{(depth\ 2 - depth\ 1)^2 + \left(\sqrt{area\ 1} - \sqrt{area\ 2}\right)^2} \quad \text{(Eq. 3)}$$

Where depth 1 and 2 refer to the water depth of the top and bottom depth contours, and area 1 and 2 represent the planar areas at the top and bottom depth contours. This method assumes that the lakebed follows a linear slope between the bounding depth contours, so it is likely an underestimate of the true area of the sediment surface. After determining the lakebed area corresponding to each sampling site, we multiplied this area by the flux rates and then summed across all three load estimates for the total load for that sampling event. To propagate the uncertainty of this estimate, we added the standard error of the mean values in quadrature.

All data are available in Albright and Wilkinson (2021). All analyses were completed in R version 3.6.0 (R Core Team, 2019) using the sf (Pebesma, 2018), spData (Bivand and others 2021), fGarch (Wuertz and others 2020), robCompositions (Filzmoser and others 2018), and vegan packages (Oksanen and others 2019).

RESULTS

Physiochemical Conditions

Water column chemistry and thermal structure varied across sampling sites and over the course of the year (Table 1). At the shallow site, the water column remained mixed throughout the open water season and the sediment-water interface remained oxic (dissolved oxygen range 5.4-10.2 mg L^{-1}). At the intermediate and deep sites, thermal stratification first developed after ice-off. Intermittent stratification continued through late summer, after which the water column was mixed at both sites. The sediment-water interface at the intermediate depth site remained oxic throughout the study period (dissolved oxygen range 4.8-12.6 mg L^{-1}), but the deep site experienced periodic hypoxia (dissolved oxygen range 0.3-8.7 mg L^{-1}). On the day of the late summer sampling (DOY 223), a derecho passed over the lake, prompting a mixing event, as evidenced by an isothermal water column at all sampling sites. Following the derecho, the relative contribution of inorganic solids to the total suspended solids pool was much greater than any other point throughout the year in both surface and bottom waters, suggesting that the storm resulted in sediment disturbance and a well-mixed water column (Supplementary Table S1). Hypolimnetic P concentrations followed a similar seasonal pattern across sampling sites (Figure 2). At the deep and intermediate sites hypolimnetic TP concentrations remained stable between under-ice sampling (DOY 39) and early spring (DOY 117). Hypolimnetic concentrations of both TP and SRP then increased from spring through late summer, peaking at 318.0 to 370.9 µg L^{-1} and 116.3 to 168.5 µg L^{-1}, respectively, before declining in autumn. Although these nutrient concentrations are quite high, the dynamics of P in the water column in 2020 are consistent with concentrations and seasonal patterns previously measured in GVL (Supplementary Figure S1).

Sediment P fluxes

Sediment P flux rates varied substantially among sampling sites and across seasons (Figure 2, Supplementary Table S2). Flux rates were most variable over time at the deep site; however, these profundal sediments were a consistent source of P to the overlying water from winter to mid-summer (DOY 39, 117, 181), and then became a moderate sink or source of P in the late summer and autumn (DOY 223, 298). Sediments from the intermediate depth site retained P under ice cover (DOY 39), but released P in spring and late summer (DOY 117, 223). The shallow site followed a similar seasonal pattern with sediment P release in spring and late summer (DOY 117, 223) and negligible fluxes in mid-summer and autumn (DOY 181, 298). Overall, the highest rates of P release occurred at the shallow and intermediate sites in late summer (DOY 223) and in winter and mid-summer (DOY 39, 181) at the deep site.

Over the course of the year, sediment P release occurred under a broad range of dissolved oxygen concentrations at the sediment-water interface (Figure 3, Table 1). At the deep site, nearly anoxic conditions were associated with elevated rates of P release in winter and mid-summer (DOY 39, 181; dissolved oxygen 1.1 and 0.3 mg L^{-1}, respectively). However, most of the observed instances of P release occurred when oxygen was available at the sediment-water interface. For example, sediments across all three sampling sites released P under oxic conditions in spring (DOY 117; dissolved oxygen range 5.8-9.4 mg L^{-1}), and high rates of oxic P release occurred at the intermediate and shallow sites in late summer (DOY 223; dissolved oxygen 4.8 and 7.2 mg L^{-1}, respectively). The effect of dissolved oxygen availability on sediment P flux rates differed between the deep site and more shallow sampling sites, and elevated P release rates were observed under both oxic and anoxic conditions.

The shape of the distribution of sediment P flux rates over the course of 2020 provides evidence of hot spots and hot moments of sediment P release in GVL. The distribution of P flux rates was centered near 0 mg P m^{-2} day^{-1} with the majority of the rates falling between -10 and 10 mg P m^{-2} day^{-1} (Supplementary Figure S2). The first statistical moment, or mean, of the distribution was 3.4 mg P m^{-2} day^{-1}. The distribution was moderately positively-skewed (third standardized statistical moment $m_3 = 0.818$) due to five high release rates (range 16.2-23.6 mg P m^{-2} day^{-1}). The four highest of these points were classified as statistical outliers. The high release rates were from the deep sampling site in winter and mid-summer (DOY 39, 181) as well as fluxes in late summer (DOY 223) from the intermediate and shallow sites (Supplementary Figure S3). Subsampling the dataset to exclude the five highest flux rates resulted in an approximately symmetric distribution ($m_3 = 0.462$; Supplementary Table S3). The mean flux rate with the five highest rates excluded was 1.2 mg P m^{-2} day^{-1}, which is almost a third of the mean flux rate for the whole distribution. The presence of high flux rates that skew the distribution indicate hot spots and hot moments of sediment P release.

Sediment P Composition

To understand spatiotemporal variation in sediment P fluxes, we also measured changes in the sediment P pool, the slow variable, across seasons and sampling sites. Redox-sensitive P was the dominant pool of mobile P found in the reservoir sediments constituting an average of 40.9-51.3 percent of the total P pool across sites (Supplementary Figure S4). The concentrations of all mobile sediment P species were dynamic over time across the reservoir. Redox-sensitive P concentrations decreased over the course of the year at the shallow site. At the intermediate depth site, redox-sensitive P concentrations increased from winter to spring (DOY 39-117), declined through late summer (DOY 223), and increased until autumn (DOY 298). Redox-sensitive P at the deep site declined from winter through late summer (DOY 39-223), before increasing through autumn (DOY 223-298; Figure 4A).

Overall, concentrations of labile organic P increased from spring to autumn at all study sites, except for slight declines between mid-summer and late summer (DOY 181-223) at the intermediate and shallow sites (Figure 4B). Aluminum-bound P concentrations declined from spring through autumn at the shallow site. At the intermediate depth site, concentrations increased from winter to spring (DOY 39-117), declined through late summer (DOY 223), and then increased again. At the deep site, aluminum-bound P followed an inverse pattern to that of redox-sensitive P, increasing from winter through late summer (DOY 39-223) and decreasing from late summer to autumn (DOY 223-298; Figure 4C). Temporal patterns in loosely-bound P varied across sites with declines over the study period at the shallow site, a gradual increase over time at the intermediate site, and steady concentrations at the deep site except for an increase from late summer to autumn (DOY 223-298; Figure 4D).

We used PCA as part of a compositional data analysis to explore spatiotemporal variation in overall sediment P composition. The compositional analysis was defined by the concentrations of loosely-bound, redox-sensitive, aluminum-bound, and labile organic P (Figure 4E). The first principal component (PC1) explained 76.77% of the variation in the dataset and was highly correlated with loosely-bound and redox-sensitive P content. The second principal component (PC2) explained (14.35%) of the variation and was more closely associated with labile organic P content. The first two principal components explained 91.12% of the variance in the dataset. Overall, sediment samples from the shallow site had lower loosely-bound and redox-sensitive P content, whereas these species were more prevalent in the deep site sediments. The composition of the sediments from the intermediate site fell between that of the deep and shallow sites. Over the course of the study period, sediment composition from all study sites generally decreased in loosely-bound and redox-sensitive P content and increased in labile organic P content.

Total P Load

We estimated daily sediment P loads for each sampling event by scaling the measured flux rates to representative areas of the lakebed to better understand the ecosystem-scale consequences of the P fluxes. The estimated total P load across the lakebed varied over time, with higher loads occurring under oxic conditions in spring and late summer (DOY 117, 223; Figure 5, Table 2). The greatest total P load occurred in late summer (DOY 223) due to high flux rates from the shallow and intermediate sites under oxic conditions (Figure 3). Oxic conditions were also associated with high total P loads in spring (DOY 117), when low P release rates across all sampling sites resulted in a substantial total P load due to the large area of the lakebed releasing P. In contrast, high rates of sediment P release under anoxic conditions at the deep site in winter and mid-summer (DOY 39, 181) did not translate into a high total P load due to the small area of lakebed involved. The greatest P loads were associated with aerobic sediment P release across a broad area of the lakebed. The seasonal trend in the estimated total P load mirrors the observed time series for hypolimnetic TP and SRP (Figure 2).

DISCUSSION

There was clear evidence of hot spots and hot moments of sediment P release in GVL over the course of 2020. These elevated rates of sediment P flux occurred in late summer at the shallow and intermediate depth sites as well as in winter and mid-summer at the deep site. While the single highest rate of sediment P release occurred under anoxic conditions, the other elevated flux rates at the shallow and intermediate sites happened when dissolved oxygen was available at the sediment-water interface. Other studies of hypereutrophic reservoirs have also observed aerobic sediment P release associated with intense algal production and P mobilization during decomposition of sediment organic matter (Song and Burgin 2017, McCarty 2019). As a hypereutrophic waterbody, GVL also experiences severe algal blooms throughout the summer months, so it is likely that microbial decomposition of algal detritus fueled the observed aerobic P release.

In addition to aerobic P mobilization from sediment organic matter, a severe storm disturbance on the late summer sampling date could have further exacerbated internal loading at the shallow and intermediate sites. The late summer sampling event occurred immediately following a derecho, which mixed the reservoir water column and disturbed sediments. Sediment resuspension has been shown to increase diffusive P flux from sediments into the overlying water, even after the sediments have settled following the disturbance (Tammeorg and others 2016). Resuspension dilutes the pore water near the sediment surface, prompting diffusion of soluble P from deeper within the sediment profile and thus enhancing diffusive P fluxes into the water column. It is likely that the high rates of aerobic P release observed at the shallow and intermediate sites in late summer resulted from both P mineralization from organic matter and sediment disturbance brought on by the storm event. Bottom water TP and SRP concentrations also peaked at this time, indicating that these high flux rates influenced whole-reservoir P dynamics.

The highest rates of P flux from the deep site occurred under ice cover and in mid-summer under nearly anoxic conditions at the sediment-water interface. Profundal sediment P release during summer anoxia has been recorded in many other waterbodies and attributed to reductive dissolution of redox-sensitive P minerals (Mortimer 1941, Nowlin and others 2005, Kowalczewka-Madura and others 2019). However, winter measurements of sediment P fluxes are uncommon (Cavaliere and others 2020). Of those measurements that have been made under ice, many studies report low flux rates in the winter (Orihel and others 2017), while others have measured substantial winter loading (Reedyk and others 2001, North and others 2015). Our results provide further evidence that mobilization and release of sediment P is still possible under ice cover. Despite the high flux rates measured under ice, hypolimnetic TP concentrations did not increase from winter to the next sampling event in spring. The winter P fluxes may not have been sustained long enough to cause a noticeable increase in water column P. Alternatively, the P released under ice-cover could have been exported downstream before the spring sampling event or diluted during ice melt (Cavaliere and others 2020). The relative importance of winter internal loading is likely system-specific, but to assume that winter P fluxes are negligible risks biasing estimates of annual internal loading.

Sediment core incubations are a common tool for measuring sediment P flux rates (Orihel and others 2017); however, the approach also has limitations (Oghdal and others 2014). The main assumption when using core incubations to quantify sediment flux dynamics is that the conditions in the core are representative of the conditions in the lake. In an effort to meet this assumption, we incubated cores at ambient temperature and oxygen conditions at the time of collection, monitoring the temperature, dissolved oxygen, and pH daily in the cores. We also used measurements from replicate cores and multiple days of incubation to estimate daily mean flux rates at a site for a given sampling event in order to capture small-scale spatiotemporal variability in the estimate while comparing across larger spatial and temporal scales. Additionally, we limited our incubations to 3.5 days in order to minimize artifacts that can occur in long-term incubations such as the depletion of organic matter or other key nutrients. Finally, we compared our core incubation-based flux measurements to TP dynamics in the reservoir as another way to verify that the qualitative patterns we observed in flux rates matched the changes in TP concentration measured in the reservoir. These strategies combined provide confidence that the broad-scale spatiotemporal patterns in sediment P flux we measured in GVL reflect the dynamics occurring across sites and seasons in the ecosystem.

Sediment P Composition Controls Flux Response to Dissolved Oxygen

Over the course of the year, we measured internal P loading under a wide range of dissolved oxygen concentrations at the sediment-water interface. High P flux rates occurred under nearly anoxic conditions at the deep site and oxic conditions at the shallower sampling sites. In order to understand why sediment P fluxes responded differently to dissolved oxygen conditions across space and time, we measured the chemical composition of the sediment P pool. We hypothesized that this slow variable shapes how fluxes respond to external drivers that alter dissolved oxygen availability. Spatiotemporal variation in sediment P composition corresponded to variation in sediment P flux rates due to two disparate mechanisms: oxic conditions liberated P from labile organic materials and anoxic conditions mobilized redox-sensitive P species. The dominance of aerobic versus anaerobic internal loading shifted over time and space in the study reservoir, but both processes were important pathways for P recycling between sediments and the overlying water.

At the deep site of the reservoir, change in redox-sensitive P concentrations mirrored P flux rates over time. Redox-sensitive P declined steadily from winter to mid-summer, and then sharply decreased (35% decrease) from mid- to late summer. The mid-summer sampling event was a hot spot-hot moment of P release from the profundal sediments that coincided with hypolimnetic anoxia at the deep site. The decline in redox-sensitive P from mid- to late summer suggests that the high flux rates in mid-summer were the result of reductive dissolution of redox-sensitive P minerals under anoxic conditions. Concentrations of labile organic P in the sediments generally increased over the course of the year at all sampling sites. However, declines were measured at the deep and intermediate sites from winter to spring, suggesting that the aerobic release observed in spring was due to the mineralization of labile organic P. From mid-summer to late summer, labile organic P also declined at the shallow and intermediate sites, indicating that the elevated rates of aerobic P release measured at these sites in late summer resulted from P mineralization following decomposition of labile organic materials.

Our hypothesis that there are hot spots and hot moments of internal loading resulting from interactions between sediment P composition and biogeochemical conditions at the sediment-water interface was supported in our study reservoir. We found that anoxic conditions can trigger the rapid mobilization and release of P from redox-sensitive P pools regardless of water temperature. We also measured P release originating from labile organic materials under aerobic conditions and found that these fluxes were enhanced following a storm disturbance. Our findings underscore the importance of considering both aerobic and anaerobic pathways of internal loading, especially in productive waterbodies. Our work supports the idea of a "perpetual cycle of internal P loading" in hypereutrophic waterbodies, as proposed by Song and Burgin (2017). The perpetual cycle describes a positive feedback loop that develops as lakes become increasingly eutrophic. Increased algal production enhances inputs of detritus to the sediments, producing a large pool of sediment labile organic P that is susceptible to aerobic release (Baines and Pace 1994, Frost and others 2019). Sediment P release may then occur under both anoxic and oxic conditions. High internal P loads sustain frequent algal blooms, the detritus of which further fuels aerobic sediment P release via decomposition and mineralization. This positive feedback loop likely introduces hysteresis to maintain waterbodies in a hypereutrophic state. Clear evidence of sediment P release under both oxic and anoxic conditions in GVL indicates that the reservoir has entered this proposed cycle in which both anaerobic and aerobic internal loading will continue to fuel intense algal blooms.

Scaling Fluxes to the Whole Ecosystem

A hot spot-hot moment is defined as having a disproportionate influence on elemental cycles at the ecosystem-scale (McClain and others 2003). As such, we scaled measured P flux rates to representative areas of the lakebed to estimate P loads and determine how the fluxes we classified as hot spots-hot moments actually influenced reservoir-wide internal loading. Hot spots and hot moments of aerobic P release from the shallow and intermediate depth sites in late summer produced the greatest total sediment P load to the reservoir over the study period. This substantial P load resulted from both the high flux rates and the broad spatial extent of sediments releasing P at this time. In contrast, high rates of P release from the deep site in winter and mid-summer did not result in large total P loads due to the small area of lakebed represented by the deep site as well as sediment P retention at other sampling sites. The scaling results further illustrate how even low rates of P release can result in elevated total P loads if sustained over the entire lakebed. Specifically, we found that low rates of P release across all sampling sites in spring resulted in a high total P load.

The biological relevance of these P loads varied with the timing and location of sediment P release. The spring P load occurred at an ideal time and location to fuel early summer algal blooms. Previous work has shown that GVL is strongly P-limited in early spring (Butts and others, personal communication). Additionally, a large proportion of the lakebed releasing P at this time was in direct contact with the mixed surface layer, so released P would be readily available for algal uptake. The substantial P load from the shallow and intermediate sites in late summer also occurred in contact with the mixed surface layer. In contrast, P loads from the deep site in winter and mid-summer are less likely to have reached the euphotic zone and to be available to algae (Tammeorg and others 2017). Overall, instances of aerobic sediment P release resulted in the greatest total sediment P loads to the reservoir and released P at relevant times and locations for algal uptake.

Focusing on rates alone may not be sufficient to understand how extreme values of biogeochemical fluxes actually effect ecosystem structure and function. It is essential to evaluate the biological relevance of observed rates and scale measurements to the whole system. At the same time, scaling measurements from a single sampling station to an area of the lakebed is fraught with uncertainty. However, we took a conservative approach in assigning representative areas of the lakebed. We also took care in accurately describing the reservoir basin geometry and calculating sediment surface area. As such, we have produced conservative estimates of sediment P loads that can be used to evaluate the ecosystem effects of spatiotemporal variation in P fluxes. Other studies have scaled discrete measurements of sediment P fluxes to larger areas of the lakebed, generally based on waterbody surface area (Scicluna and others 2015, Noffke and others 2016). Our approach to characterizing basin geometry allows for more accurate estimates of sediment surface area and thus scaling at finer spatial resolutions based on water depth.

Conclusions

Effective management of freshwater eutrophication in lakes and reservoirs requires a quantitative and mechanistic understanding of internal P loading (Søndergaard and others 2013, Schindler and other 2016). The high spatiotemporal variability in sediment P flux rates in GVL was the result of the slowly changing composition of the sediment P pool interacting with redox conditions controlled by external drivers. Our understanding of internal P loading in our study reservoir would have been very different had we only sampled at one site or in one season. Our findings demonstrate that the magnitude and mechanisms of internal P loading cannot be understood without capturing both seasonal and spatial variation in fluxes as well as the composition of the sediment P pool as a slowly changing variable. Additionally, quantifying rates to characterize hot spots and hot moments alone would have been insufficient in identifying the main sources and mechanisms of P release at the ecosystem-scale. Internal loading was dominated by oxic release in the shallow areas despite high release rates during anoxia at the deep site. These findings illustrate how focusing solely on high rates without the context of the whole ecosystem could lead to the misidentification of the dominant biogeochemical mechanisms at play and hamper eutrophication management efforts.

Acknowledgements

This research was supported by the Iowa Water Center's Graduate Student Supplemental Research Competition. Albright was supported by the National Science Foundation Graduate Research Fellowship Program under Grant No. DGE-1747503. Any opinions, findings, and conclusions or recommendations expressed in this material are those of the authors and do not necessarily reflect the views of the National Science Foundation. Support was also provided by the Graduate School and the Office of the Vice Chancellor for Research and Graduate Education at the University of Wisconsin-Madison with funding from the Wisconsin Alumni Research Foundation. Wilkinson was supported by the National Science Foundation Division of Environmental Biology grant #1942256.

Data Availability Statement

The data supporting the conclusions are publicly available in Albright and Wilkinson (2021), under a Creative Commons Attribution license (CC-BY). The analysis code is available in the Github repository https://github.com/AlbrightE/GVL_Internal_P_Cycling, which will be archived on Zenodo after manuscript acceptance.

TABLES

Table 1. Thermal stratification and oxygen conditions at the sediment-water interface.

				Sediment-Water Interface Conditions		
DOY	Season	Site	Water Column Thermal Structure	Temperature (°C)	DO (mg L^{-1})	DO Saturation (%)
39	Winter	Intermediate	Stratified	3.2	12.6	94.3
		Deep	Stratified	4.2	1.1	8.6
117	Spring	Shallow	Isothermal	14.6	9.4	92.5
		Intermediate	Stratified	14.1	8.9	86.4
		Deep	Stratified	11.9	5.8	54.3
181	Mid-Summer	Shallow	Isothermal	26.5	5.4	67.4
		Intermediate	Isothermal	26.3	6.3	78.0
		Deep	Isothermal	24.2	0.3	3.3
223	Late Summer	Shallow	Isothermal	26.1	7.2	88.7
		Intermediate	Isothermal	25.4	4.8	58.0
		Deep	Isothermal	24.9	4.5	54.2
298	Autumn	Shallow	Isothermal	6.7	10.2	83.3
		Intermediate	Isothermal	8.1	8.7	73.7
		Deep	Isothermal	8.4	8.7	73.8

Table 2. Estimated mean P load by site and total load.

	Lakebed Information		Estimated Mean P Load ± Standard Error (kg P day^{-1})				
Site	Depth Contour	Sediment Area (m^2)	Winter	Spring	Mid-Summer	Late Summer	Autumn
Shallow	1.2-3.6 m	3,014,983.6	n.a.	6.2 ± 2.8	-0.3 ± 10.3	25.2 ± 10.1	-2.2 ± 3.4
Intermediate	3.6-5.6 m	1,593,676.1	-2.5 ± 1.7	1.9 ± 0.3	-5.8 ± 9.3	15.4 ± 13.7	0.4 ± 1.1
Deep	> 5.6 m	801,995.5	9.0 ± 5.0	1.9 ± 0.2	13.8 ± 0.9	1.9 ± 3.0	-1.2 ± 1.3
Estimated Total Load (kg Pday^{-1})			6.5 ± 1.7	10.0 ± 2.8	7.8 ± 10.3	42.5 ± 10.1	-2.9 ± 3.4

FIGURES

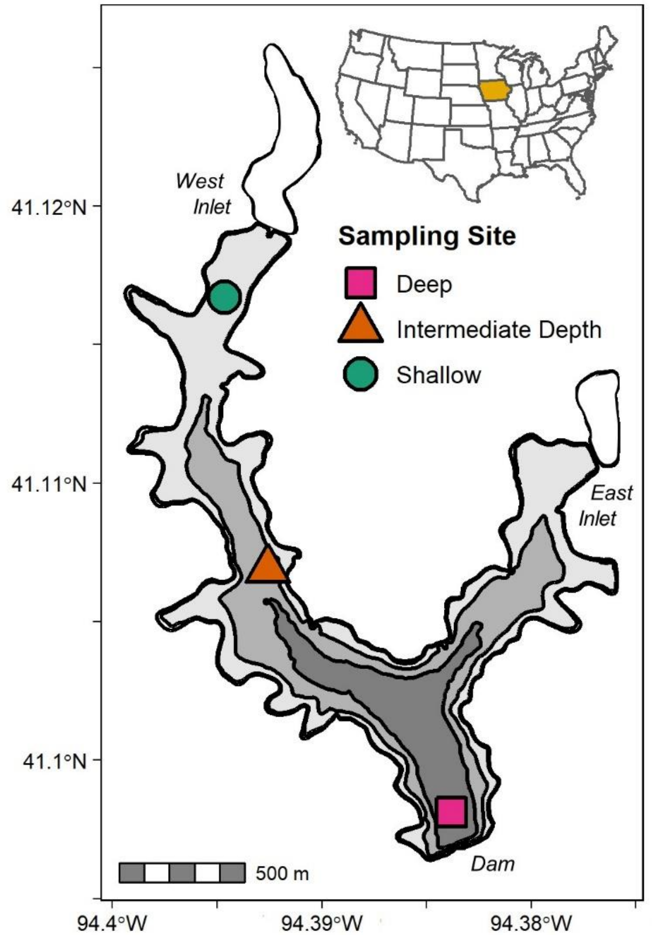

Figure 1. Sampling sites in Green Valley Lake, Iowa, USA. The three sampling sites are representative of different areas of the lakebed based on water depth. The shaded polygons illustrate these areas. The shallow site is representative of the 1.2-3.6 m depth contour. The intermediate depth site is representative of the 3.6-5.6 m interval, and the deep site is representative of the area deeper than 5.6 m.

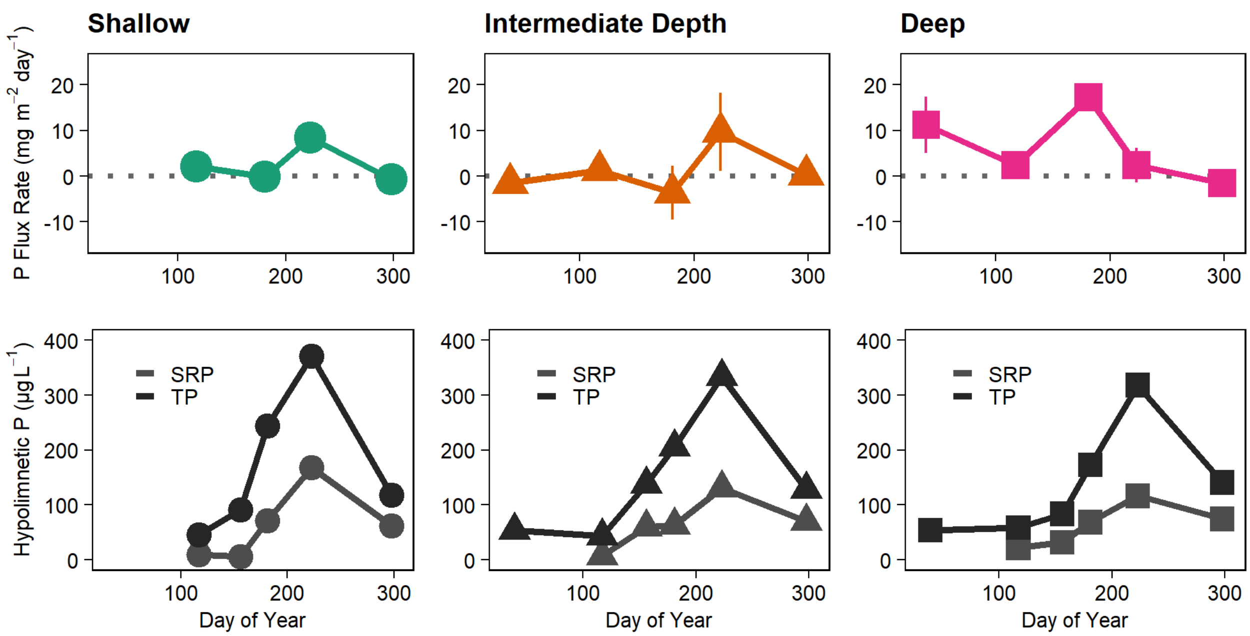

Figure 2. Sediment P flux rates and hypolimnetic P concentrations. (Top row of panels) Time series of mean sediment total P flux (± standard deviation among replicate cores) from February to October of 2020. The shallow site was not sampled in February due to unsafe ice conditions. Negative values indicate sediment P retention while positive values show P release. (Bottom row of panels) Time series of hypolimnetic total P (TP) and soluble reactive P (SRP) concentrations for each sampling site over the study period.

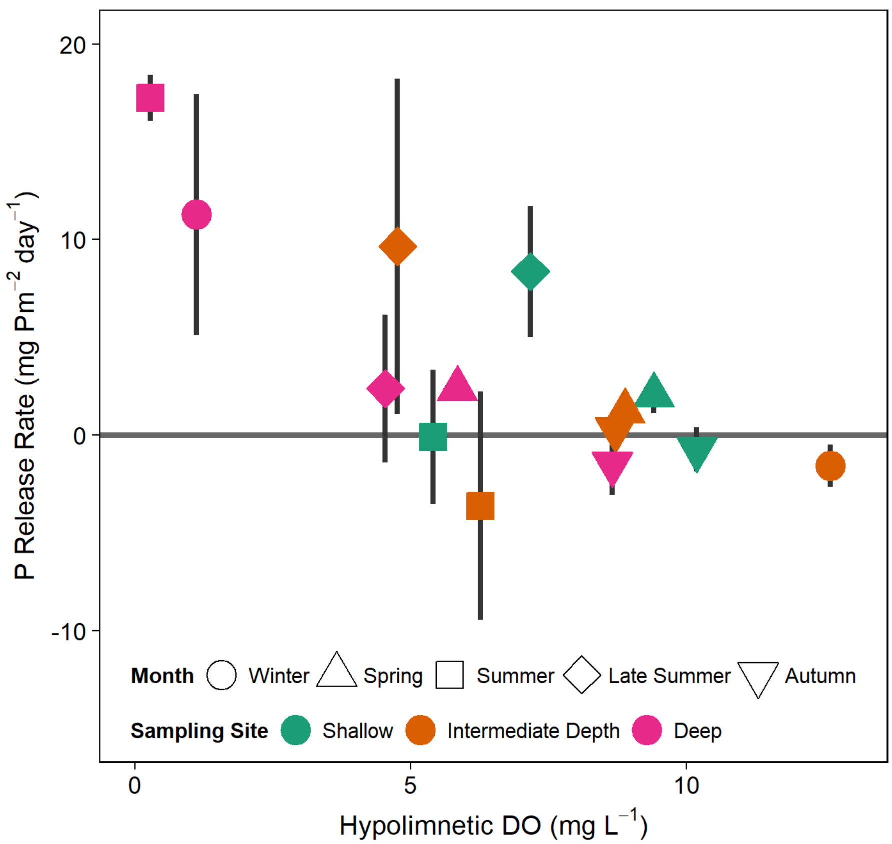

Figure 3. Mean sediment P flux rates (± standard deviation among replicate cores) across the range of observed hypolimnetic dissolved oxygen concentrations.

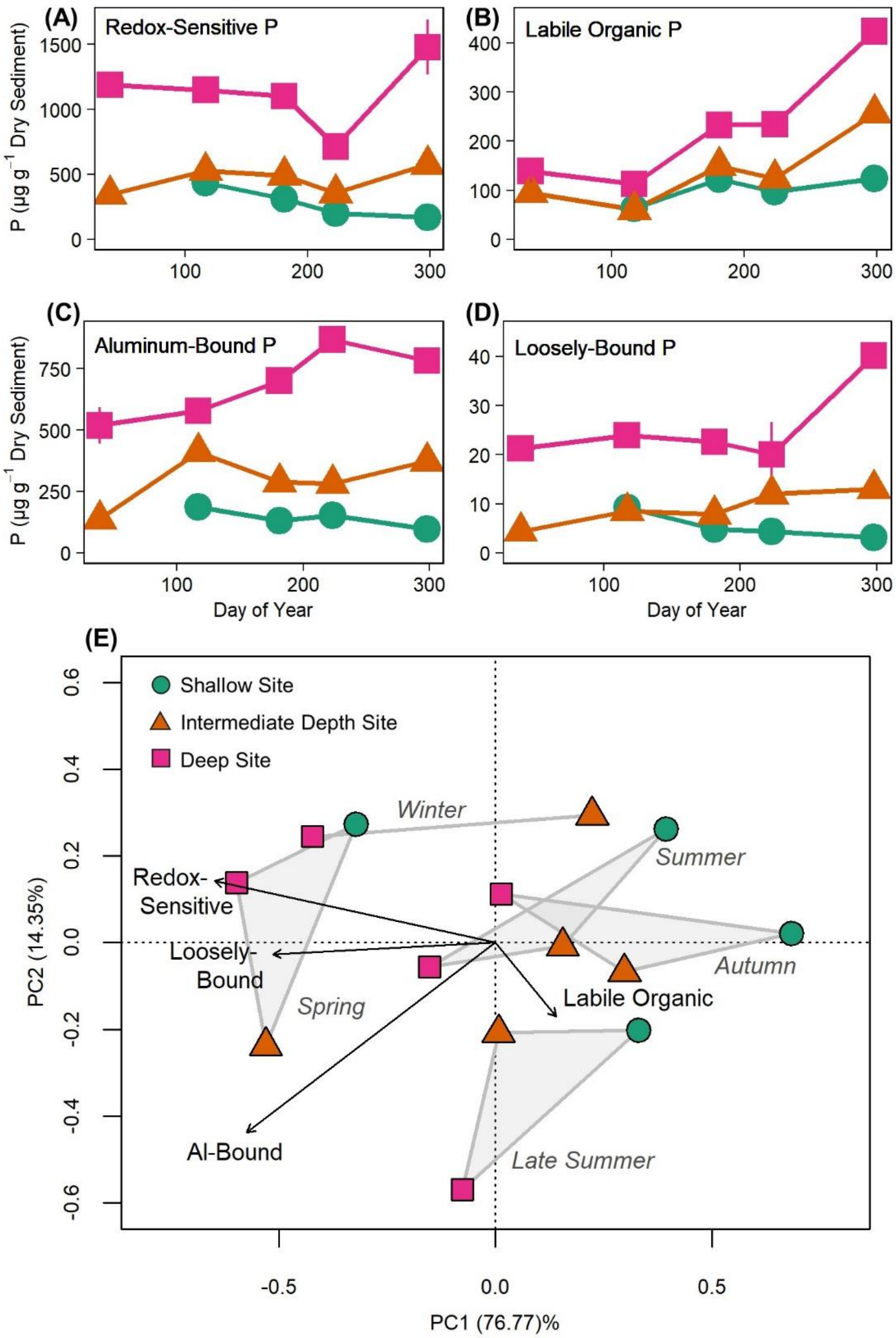

Figure 4. Spatiotemporal variation in mobile sediment P species. Time series of mean (± standard deviation of replicate samples) (A) redox-sensitive P, (B) labile organic P, (C) aluminum-bound, and (D) loosely-bound P concentrations across sampling sites and over the course of the year. (E) PCA biplot based on a compositional data analysis of sediment P pools over the course of the year.

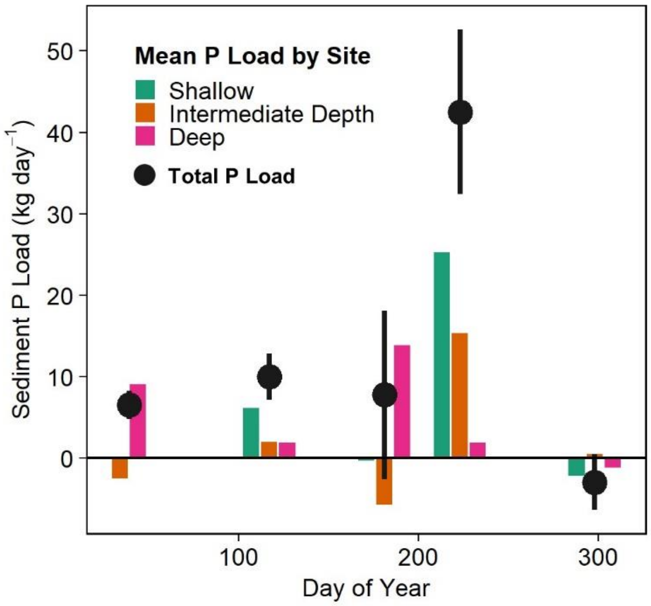

Figure 5. Estimated mean P load at the time of sampling by site (bars) and total load across the lakebed (points; error bars are ± standard error). Bar plots show the mean, estimated P load for each sampling site at the time of sampling. Points represent the sum of the estimated loads across the lakebed.

References

1. Albright EA, Wilkinson GM. 2021. Spatiotemporal variation in internal phosphorus loading, sediment characteristics, water column chemistry, and thermal mixing in a hypereutrophic reservoir in southwest Iowa, USA (2019-2020) ver 1. Environmental Data Initiative. https://doi.org/10.6073/pasta/d3a70c1f0d534cca8bdebd7f7483ef38 (Accessed 2021-10-14).
2. Baines SB, Pace ML. 1994. Relationships between suspended particulate matter and sinking flux along a trophic gradient and implications for the fate of planktonic primary production. Canadian Journal of Fisheries and Aquatic Science 51: 25-36.
3. Bernhardt ES, Blaszczak JR, Ficken CD, Fork ML, Kaiser KE, Seybold EC. 2017. Control points in ecosystems: Moving beyond the hot spot hot moment concept. Ecosystems 20(4): 665–82.
4. Bivand R, Nowosad J, Lovelace R. 2021. spData: Datasets for Spatial Analysis. R package version 0.3.10.
5. Boström B, Pettersson K. 1982. Different patterns of phosphorus release from lake-sediments in laboratory experiments. Hydrobiologia 91-2 (1): 415-429.
6. Buelo CD, Carpenter SR, Pace ML. 2018. A modeling analysis of spatial statistical indicators of thresholds for algal blooms. Limnology and Oceanography Letters 3(5): 384–392.
7. Cardoso-Silva S, Ferreira PA, Figueira RCL, Silva DC, Moschini-Carlos V, Pompêo MLM. 2018. Factors that control the spatial and temporal distributions of phosphorus, nitrogen, and carbon in the sediments of a tropical reservoir. Environmental Science and Pollution Research 25: 31776–31789.

8. Carpenter SR. 2003. Regime Shifts in Lake Ecosystems: Pattern and Variation. Oldendorf/Luhe, Germany: Ecology Institute.
9. Carpenter SR, Turner MG. 2000. Hares and tortoises: Interactions of fast and slow variables in ecosystems. Ecosystems 3: 495-497.
10. Cavaliere E, Baulch HM. 2020. Winter in two phases: Long-term study of a shallow reservoir in winter. Limnology and Oceanography 66(4): 1335-1352.
11. Corfidi SF, Coniglio MC, Cohen AE, Mead CM. 2016. A Proposed Revision to the Definition of "Derecho". Bulletin of the American Meteorological Society 97: 935-949.
12. Crépin A. 2007. Using fast and slow processes to manage resources with thresholds. Environmental & Resource Economics 36: 191-213.
13. Filzmoser P, Hron K, Templ M. 2018. Applied Compositional Data Analysis with Worked Examples in R. Spring Series in Statistics. Spring International Publishing, Cham, Switzerland.
14. Forsberg C. 1989. Importance of sediments in understanding nutrient cyclings in lakes. Hydrobiologia 176/177: 263-277.
15. Frost PC, Prater C, Scott AB, Song K, Xenopoulos MA. 2019. Mobility and Bioavailability of Sediment Phosphorus in Urban Stormwater Ponds. Water Resources Research 55(5): 3680-3688.
16. Gakuruh H. 2017. Essentials of Data Analysis and Graphics Using R. https://helleng.github.io/Data_Mgt_Analysis_and_Graphics_R/Data_Analysis
17. Goff TC, Nelson MD, Liknes GC, Feeley TE, Pugh SA, Morin RS. 2021. Rapid assessment of tree damage resulting from a 2020 windstorm in Iowa, USA. Forests 12: 555.

18. Guenet B, Danger M, Abbadie L, Lacroix G. 2010. Priming effect: bridging the gap between terrestrial and aquatic ecology. Ecology 91(10): 2850-2861.

19. Guillemette F, McCallister SL, del Giorgio PA. 2013. Differentiating the degradation dynamics of algal and terrestrial carbon within complex natural dissolved organic carbon in temperature lakes. Journal of Geophysical Research: Biogeosciences 118: 963-973.

20. Hayes NM, Deemer BR, Corman JR, Razavi NR, Strock KE. 2017. Key differences between lakes and reservoirs modify climate signals: A case for a new conceptual model. Limnology and Oceanography Letters 2(2): 47-62.

21. Horppila J, Holmroos H, Niemistö J, Massa I, Nygrén N, Schönach P, Tapio P, Tammeorg O. 2017. Variations of internal phosphorus loading and water quality in a hypertrophic lake during 40 years of different management efforts. Ecological Engineering 103: 264-274.

22. Hudson JJ, Vandergucht DM. 2015. Spatial and temporal patterns in physical properties and dissolved oxygen in Lake Diefenbaker, a large reservoir on the Canadian Prairies. Journal of Great Lakes Research 41(2): 22-33.

23. Hupfer M, Lewandowski J. 2008. Oxygen controls the phosphorus release from lake sediments – a long-lasting paradigm in limnology. International Review of Hydrobiology 93(4-5): 415-432.

24. Jensen HS and Andersen FØ. 1992. Importance of temperature, nitrate, and pH for phosphate release from aerobic sediments of four shallow, eutrophic lakes. Limnology and Oceanography 37(3): 577-598.

25. Joshi SR, Kukkadapu RK, Burdige DJ, Bowden ME, Sparks DL, Jaisi DP. 2015. Organic matter remineralization predominates phosphorous cycling in the mid-bay sediments in the Chesapeake Bay. Environmental Science and Technology 49: 5887-5896.

26. Kimmel BL, Groeger AW. 1984. Factors controlling primary production in lakes and reservoirs: A perspective. Lake and Reservoir Management 1(1): 277-281.

27. Kleeberg A, Freidank A, Jöhnk K. 2013. Effects of ice cover on sediment resuspension and phosphorus entrainment in shallow lakes: Combining in situ experiments and wind-wave modeling. Limnology and Oceanography 58(5): 1819-1833.

28. Kowalczewska-Madura K, Gołdyn R, Bogucka J, Strzelczyk K. 2019. Impact of environmental variables on spatial and seasonal internal phosphorus loading in a mesoeutrophic lake. International Journal of Sediment Research 34(1):14–26.

29. Lukkari K, Hartikainen H, Leivuori M. 2007. Fractionation of sediment phosphorus revisited. I: Fractionation steps and their biogeochemical basis. Limnology and Oceanography: Methods 5: 433-444.

30. McCarty JA. 2019. Sediment phosphorus release in a shallow eutrophic reservoir cove. Transactions of the ASABE. 62(5): 1269-1281.

31. McClain ME, Boyer EW, Dent CL, Gergel SE, Grimm NB, Groffman PM, Hart SC, Harvey JW, Johnston CA, Mayorga E, McDowell WH, Pinay G. 2003. Biogeochemical hot spots and hot moments at the interface of terrestrial and aquatic ecosystems. Ecosystems 6(4): 301-312.

32. Mortimer C. 1941. The exchange of dissolved substances between mud and water in lakes. Journal of Ecology 29: 280-239.

33. Murphy J, Riley JP. 1962. A modified single solution method for the determination of phosphate in natural waters. Analytica Chimica Acta 27: 31-36.

34. North RL, Johansson J, Vandergucht DM, Doig LE, Liber K, Lindenschmidt K, Baulch H, Hudson JJ. 2015. Evidence for internal phosphorus loading in a large prairie reservoir (Lake Diefenbaker, Saskatchewan). Journal of Great Lakes Research 41(S2): 91-99.

35. Nowlin WH, Evarts JL, Vanni MJ. 2005. Release rates and potential fates of nitrogen and phosphorus from sediments in a eutrophic reservoir. Freshwater Biology 50(2): 301–322.

36. Ogdahl ME, Steinman AD, Weinert ME. 2014. Laboratory-determined phosphorus flux from lake sediments as a measure of internal phosphorus loading. Journal of Visualized Experiments 85: e51617.

37. Oksanen J, Blanchet FG, Friendly M, Kindt R, Legendre P, McGlinn D, O'Hara RB, Simpson GL, Peter Solymos P, Henry M, Stevens H, Szoecs E, Wagner H. 2019. vegan: Community Ecology Package. R package version 2.5-6.

38. Orihel DM, Baulch HM, Casson NJ, North RL, Parsons CT, Seckar DCM, Venkiteswaran JJ. 2017. Internal phosphorus loading in Canadian fresh waters: a critical review and data analysis. Canadian Journal of Fisheries and Aquatic Science 74: 2005-2029.

39. Ortiz DA, Wilkinson GM. 2021. Capturing the spatial variability of algal bloom development in a shallow temperate lake. Freshwater Biology, in press.

40. Pebesma, E. 2018. Simple features for R: Standardized support for spatial vector data. The R Journal 10(1): 439-446.

41. Reedyk S, Prepas EE, Chambers PA. 2001. Effects of single $Ca(OH)_2$ doses on phosphorus concentration and macrophyte biomass of two boreal eutrophic lakes over 2 years. Freshwater Biology 46(8): 1075-1087.

42. R Core Team. 2019. R: A language and environment for statistical computing. R Foundation for Statistical Computing, Vienna, Austria. https://www.R-project.org/

43. Schindler DW, Carpenter SR, Chapra SC, Hecky RE, Orihel DM. 2016. Reducing phosphorus to curb lake eutrophication is a success. Environmental Science & Technology 50(17): 8923-8929.

44. Song K, Burgin AJ. 2017. Perpetual phosphorus cycling: Eutrophication amplifies biological control on internal phosphorus loading in agricultural reservoirs. Ecosystems 20: 1483-1493.

45. Standard Methods for the Examination of Water and Wastewater. 1998. 20th Edition. Method 4500-P B.5.

46. Standard Methods for the Examination of Water and Wastewater. 1998. 20th Edition. Method 4500-P E.

47. Søndergaard M, Bjerring R, Jensen JP. 2013. Persistent internal phosphorus loading 743 during summer in shallow eutrophic systems. Hydrobiologia 710 (1): 95-107.

48. Søndergaard M, Jensen JP, Jeppesen E. 2003. Role of sediment and internal loading of phosphorus in shallow lakes. Hydrobiologia 506-509: 135-145.

49. Tammeorg O, Horppila J, Tammeorg P, Haldna, M, Niemistö J. 2016. Internal phosphorus loading across a cascade of three eutrophic basins: A synthesis of short- and long-term studies. Science of the Total Environment 572: 943-954.

50. Tammeorg O, Möls T, Niemistö J, Holmroos H, Horppila J. 2017. The actual role of oxygen deficit in the linkage of the water quality and benthic phosphorus release: Potential implications for lake restoration. Science of the Total Environment 599-600: 732-738.

51. Walker BH, Carpenter SR, Rockstrom J, Crépin A, Peterson GD. 2012. Drivers, "slow" variables, "fast" variables, shocks and resilience. Ecology and Society 17(3): 30.

52. Ward NK, Fitchett L, Hart JA, Shu L, Stachelek J, Weng W, Zhang Y, Dugan H, Hetherington A, Boyle K, Carey CC, Cobourn KM , Hanson PC , Kemanian AR, Sorice MC, Weathers KC. 2019. Integrating fast and slow processes is essential for simulating human–freshwater interactions. Ambio 48: 1169-1182.

53. Walsh JR, Corman JR, Munoz SE. 2018. Coupled long-term limnological data and sedimentary records reveal new control on water quality in a eutrophic lake. Limnology and Oceanography 64(S1): S34-S48.

54. Wuertz D, Setz T, Chalabi Y, Boudt C, Chausse P, Miklovac M. 2020. fGarch: Rmetrics - Autoregressive Conditional Heteroskedastic Modelling. R package version 3042.83.2.

Supplementary Material for

SEDIMENT PHOSPHORUS COMPOSITION CONTROLS HOT SPOTS AND HOT MOMENTS OF INTERNAL LOADING IN A TEMPERATE RESERVOIR

Ellen A. Albright[1] and Grace M. Wilkinson[1]

[1]Center for Limnology, University of Wisconsin-Madison, 680 N. Park St., Madison, WI 53706

CONTENTS OF THIS FILE

INTRODUCTION

The Supplementary Material contains additional methods text detailing analysis of suspended solids, total nitrogen, and nitrate as well as use of previous monitoring data. We provide the equations used to determine sediment phosphorus (P) flux rates as well as sediment physical characteristics and the concentrations of sediment total P and various P species. We have also provided the standard equation for determining the third statistical moment. Table S1 details surface and bottom water chemistry including total, volatile, and involatile suspended solids; total and soluble reactive P; total nitrogen; and nitrate concentrations. Table S2 reports the mean P flux rates by site and day of year, as presented in Figure 2 in the main manuscript. Table S3 demonstrates the effects of excluding high flux rates on the skewness of the P flux distribution, as quantified by the standardized third statistical moment. We included a visualization that compares 2020 epi- and hypolimnetic total P and soluble reactive P concentrations to the P dynamics from previous years (Figure S1). Figure S2 illustrates the distribution of sediment P flux rates across sampling sites and seasons, with statistical outliers noted. Figure S3 breaks down the sediment P flux rate data by site and sampling event to identify the points in space and time associated with high flux rates. Figure S4 displays the average, annual sediment P composition by sampling site. We include citations for all references included in the Supplementary Material as well as citations for additional R packages used solely for data cleaning and visualizations.

SUPPLEMENTARY METHODS TEXT

Vertical Profiles and Water Chemistry

Suspended Solids

Total suspended solids were determined by filtering a known volume of sample water through a prepared filter (0.45µm GF/C filters) and drying to a constant weight. Volatile suspended solids were determined via loss-on-ignition, and involatile solids were assumed to be the difference between volatile and total suspended solids.

Total Nitrogen and Nitrate

Subsamples were filtered (0.45µm GF/C filters) in the lab for nitrate analysis, and all samples were preserved with concentrated sulfuric acid to pH 2. Total nitrogen samples underwent digestion prior to analysis (Standard Methods 4500-N.C). Total nitrogen and nitrate were measured via second-derivative ultraviolet spectroscopy (Crumpton and others 1992, Childress and others 1999) using an HP 8453 Spectrophotometer.

Use of Previous Monitoring Data

In order to compare water column nutrient dynamics in 2020 to previous years, we used publicly-available nutrient monitoring data from the Iowa Department of Natural Resources AQuIA database (Figure S1).

Sediment P Fluxes

Eq. 1 – *Mass of P in the Overlying Water*

$$\text{Water Column Mass P (mg)} = \text{Water column [TP] (mg/L)} * (\text{Total Water Volume (L)} - \text{Replacement Water Volume (L)}) \quad (1)$$

Eq. 2 – *Mass of P in the Replacement Water*

$$\text{Replacement Water Mass P (mg)} = \text{Replacement Water [TP] (mg/L)} * \text{Replacement Water Volume (L)} \quad (2)$$

Eq. 3 – *New TP Concentration Following Addition of Replacement Water*

$$\text{New [TP] (mg/L)} = (\text{Water Column Mass P (mg)} + \text{Replacement Water Mass P (mg)}) / \text{Total Water Volume (L)} \quad (3)$$

Eq. 4 – *Daily Change in TP Concentration*

$$\Delta\ \text{[TP] (mg/L)} = \text{Water Column [TP]}_{\text{day } n}\ \text{(mg/L)} - \text{New [TP]}_{\text{day } n\text{-}1}\ \text{(mg/L)} \quad (4)$$

Sediment P Content and Composition

Additional subsamples of fresh sediment were used for analysis of physical characteristics. For each site, three replicate subsamples were dried to a constant mass and the wet and dry masses were used to determine sediment moisture content (MC). The subsamples were then combusted and weighed again to calculate organic matter content as loss-on-ignition (LOI) and estimate bulk density (Håkanson and Jansson 2002).

Eq. 1 – *Moisture Content (MC)*

$$\text{Moisture Content (\%)} = \left[\frac{(W_w - W_t) - (W_d - W_t)}{W_w - W_t}\right] \times 100 \qquad (1)$$

Where W_t is the weight of the aluminum weigh boat, W_w is the weight of the weigh boat and fresh sediment sample, and W_d is the weight of the weigh boat and dry sediment.

Eq. 2 – *Organic Matter Content as Loss-on-Ignition (LOI)*

$$\text{LOI Organic Matter Content (\%)} = \left[\frac{(W_d - W_t) - (W_a - W_t)}{W_d - W_t}\right] \times 100 \qquad (2)$$

Where W_a is the weight of the weigh boat and the ashed sediment after combustion.

Eq. 3 – *Bulk Density*

$$\text{Bulk Density } \left(\text{g/cm}^3\right) = \frac{260}{100 + 1.6 \times \left[\text{MC} + \left(\frac{\text{LOI}}{100 \times (100\text{-MC})}\right)\right]} \qquad (3)$$

Eq. 4 – *Dry Mass Equivalent of Fresh Sediment Used*

$$\text{Dry Mass Equivalent (g)} = \text{Mass Fresh Sediment (g)} \times (100 - \text{MC}) \qquad (4)$$

Eq. 5 – *Loosely-Sorbed and Pore Water P*

$$\text{Loosely-Bound P (mg P/g dry sediment)} = \frac{\text{Concentration TP (mg/L)} \times \text{Solution Volume (L)}}{\text{Dry Mass Equivalent of Sediment Used (g)}} \qquad (5)$$

The concentration of TP used should reflect the average of lab duplicates, corrected for any dilutions. The solution volume should equal the total amount of 0.46 M NaCl extractant and rinse solutions (0.1 L total). The dry mass equivalent of the fresh sediment used is estimated based on MC (Eq. 4) and will be the same for the calculations of each subsequent extraction.

Eq. 6 – *Redox-Sensitive P*

$$\text{Redox-Sensitive P (mg P/g dry sediment)} = \frac{\text{Concentration TP (mg/L)} \times \text{Solution Volume (L)}}{\text{Dry Mass Equivalent of Sediment Used (g)}} \qquad (6)$$

The concentration of TP used should reflect the average of lab duplicates, corrected for any dilutions. The solution volume should equal the total volume of the 0.11 M bicarbonate – 0.1 M sodium dithionate solution and the rinse solutions (0.2 L total).

Eq. 7 – *Aluminum-Bound P*

$$\text{Al-Bound P (mg P/g dry sediment)} = \frac{\text{Concentration SRP (mg/L)} \times \text{Solution Volume (L)}}{\text{Dry Mass Equivalent of Sediment Used (g)}} \quad (7)$$

The concentration of SRP used should reflect the average of lab duplicates, corrected for any dilutions. The solution volume should equal the total volume of 0.1 M NaOH used and the rinse solutions (0.150 L total).

Eq. 8 – *Labile Organic P*

$$\text{Labile Organic P (mg P/g dry sediment)} = \left[\frac{\text{Concentration TP (mg/L)} \times \text{Solution Volume (L)}}{\text{Dry Mass Equivalent of Sediment Used (g)}}\right] - \text{Al-Bound P} \quad (8)$$

The concentration of TP from the supernatant should first be corrected for the volume of NaOH and rinse solutions used (0.15 L total) and the sediment mass. This value represents the concentration of aluminum-bound and total labile organic P in the sediment pellet. The concentration of labile organic P is calculated as the difference between this value and the Al-bound P concentration (Eq. 7).

Eq. 9 – *Total P*

$$\text{Total P (mg P/g dry sediment)} = \frac{\left[\text{Concentration TP}\left(\frac{\text{mg}}{\text{L}}\right) \times \frac{\text{(Post pH (g)-Tare (g))}}{\text{(Pre pH (g)-Tare (g))}}\right] \times \text{Dilution Volume (L)}}{\text{Dry Mass of Sediment Used (g)}} \quad (9)$$

The concentration of TP used should reflect the average of lab duplicate measures and must be corrected for the pH adjustment. The corrected TP concentration can then be corrected for the volume to which the sample was diluted after boiling (0.05 L) and the mass of dry sediment.

Statistical Analyses

Eq. 1 – *Skewness, third statistical moment (m_3)*

$$m_3 = \frac{\sum(x-\mu)^3}{n} \quad \text{(Eq. 1)}$$

The third statistical moment quantifies skewness and can be standardized by dividing by the cube of the standard deviation. Perfectly symmetric distributions have an m3 value of zero.

Table S1. Epi- and hypolimnetic water chemistry by site and sampling event

			Suspended Solids (mg L^{-1})			Phosphorus (µg L^{-1})		Nitrogen (mg L^{-1})	
DOY	Site	Water Column	TSS	VSS	ISS	TP	SRP	TN	No_x
39	Intermediate	Surface	NA	NA	NA	49.6	NA	NA	NA
		Bottom	7.5	4.5	3.0	54.2	NA	NA	0.4
	Deep	Surface	NA	NA	NA	42.7	NA	NA	NA
		Bottom	5.5	NA	NA	53.9	NA	NA	0.3
117	Shallow	Surface	1.1	NA	NA	39.5	7.1	1.0	0.7
		Bottom	9.5	NA	NA	45.6	9.3	0.9	0.7
	Intermediate	Surface	12.2	NA	NA	33.7	5.5	0.8	0.6
		Bottom	3.0	NA	NA	43.7	7.3	0.8	0.7
	Deep	Surface	5.5	NA	NA	35.0	1.9	0.6	0.6
		Bottom	1.5	NA	NA	58.5	22.0	0.7	0.4
181	Shallow	Surface	36.7	25.7	11.0	251.2	66.9	1.3	0.1
		Bottom	30.3	18.7	11.7	243.6	71.6	1.0	0.1
	Intermediate	Surface	22.0	17.0	5.0	327.4	63.0	0.9	0.1
		Bottom	22.1	15.3	6.8	206.0	63.3	1.0	0.0
	Deep	Surface	15.0	13.0	2.0	178.7	59.6	0.7	0.1
		Bottom	16.4	14.8	1.7	173.0	68.7	0.9	0.1
223	Shallow	Surface	51.0	28.5	22.5	376.4	173.1	1.3	0.1
		Bottom	43.5	21.0	22.5	370.9	168.5	1.3	0.1
	Intermediate	Surface	41.0	29.5	11.5	343.6	134.0	1.4	0.1
		Bottom	40.0	20.0	20.0	334.0	131.2	1.2	0.1
	Deep	Surface	38.0	19.0	19.0	330.3	116.6	1.1	0.1
		Bottom	32.0	17.5	14.5	318.0	116.3	1.3	0.1
298	Shallow	Surface	6.6	NA	NA	115.9	61.6	1.0	0.3
		Bottom	3.2	NA	NA	118.1	62.3	0.9	0.3
	Intermediate	Surface	8.0	NA	NA	131.6	69.2	1.0	0.3
		Bottom	17.6	NA	NA	128.4	69.7	1.0	0.3
	Deep	Surface	6.2	NA	NA	138.4	71.0	1.0	0.2
		Bottom	2.4	NA	NA	141.1	74.3	1.0	0.3

Surface water samples were taken 0.25 m below the surface and bottom water samples were taken 0.5 m above the sediment-water interface. Suspended solid constituents measured include total (TSS), volatile (VSS) and involatile (ISS).

Table S2. Mean P flux rates across sampling sites and seasons.

	Mean P Flux Rate ± Standard Error (mg P m^{-2} day^{-1})				
Sampling Site	***February***	***April***	***June***	***August***	***October***
Shallow		2.0 ± 0.9	-0.1 ± 3.4	8.4 ± 3.4	-0.7 ± 1.1
Middle	-1.6 ± 1.1	1.2 ± 0.2	-3.6 ± 5.8	9.6 ± 8.6	0.3 ± 0.7
Deep	11.3 ± 6.2	2.4 ± 0.3	17.2 ± 1.2	2.4 ± 3.8	-1.5 ± 1.6

Values indicate the mean P flux rate ± standard error across three replicate sediment cores. Blue cells indicate sediment P retention, orange cells corresponded to sediment P release, and either retention or release may have occurred during times indicated in grey.

Table S3. Influence of excluding high flux rates on distribution skewness.

Dataset Subsample	***Standardized Third Statistical Moment (m_3)***	***Distribution Shape***
Full dataset	0.818	Moderately positively skewed
Exclude highest flux	0.734	Moderately positively skewed
Exclude 2 highest fluxes	0.718	Moderately positively skewed
Exclude 3 highest fluxes	0.666	Moderately positively skewed
Exclude 4 highest fluxes	0.584	Moderately positively skewed
Exclude 5 highest fluxes	0.462	approximately symmetric

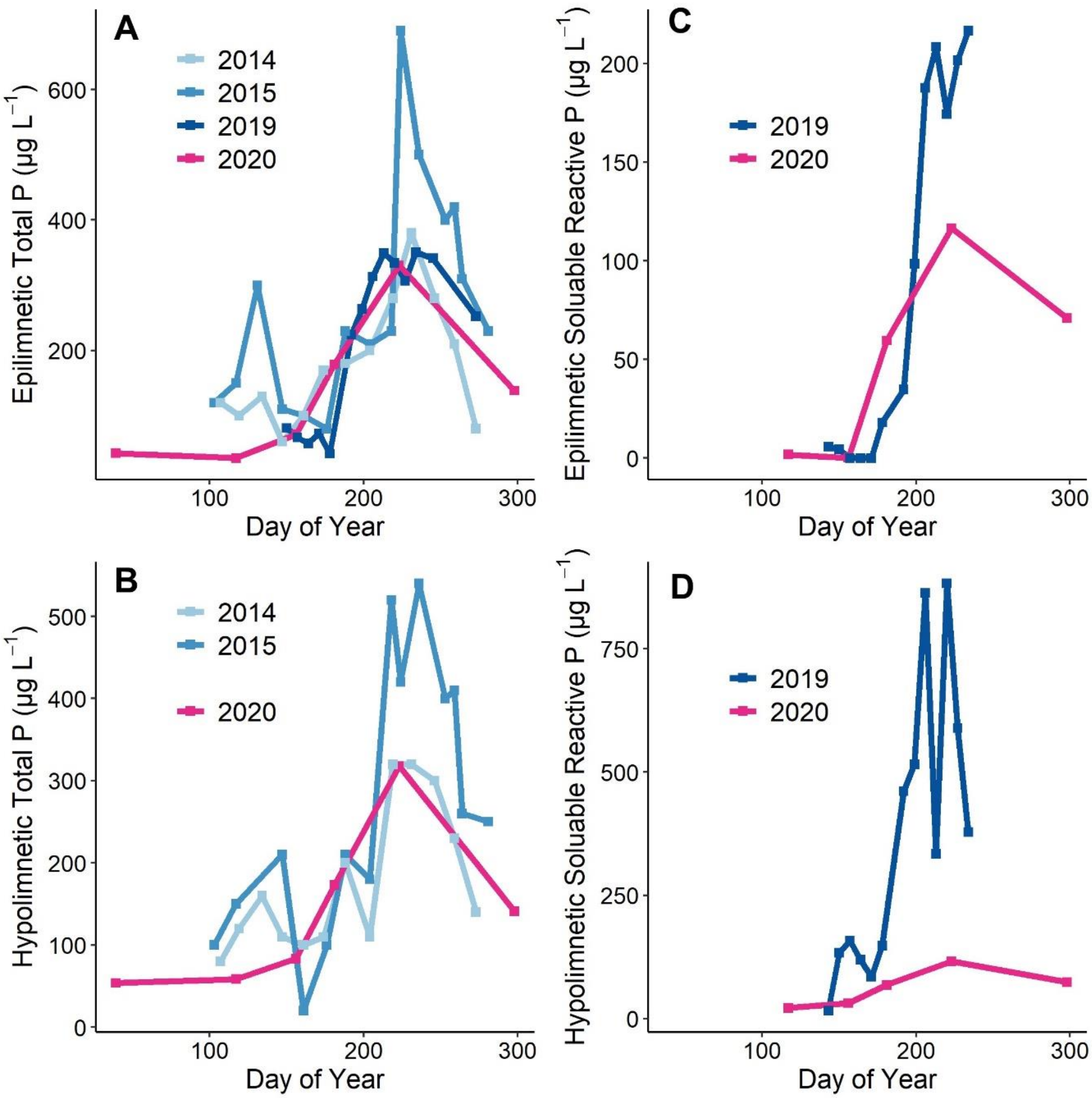

Figure S1. *Comparing 2020 epi- and hypolimnetic P dynamics to previous years (2014, 2015, 2019).* The 2020 P dynamics followed similar seasonal trends as past years in epilimnetic TP (A) and hypolimnetic TP (B) concentrations. Epilimnetic and hypolimnetic SRP concentrations were higher in 2019 than in 2020 (C-D).

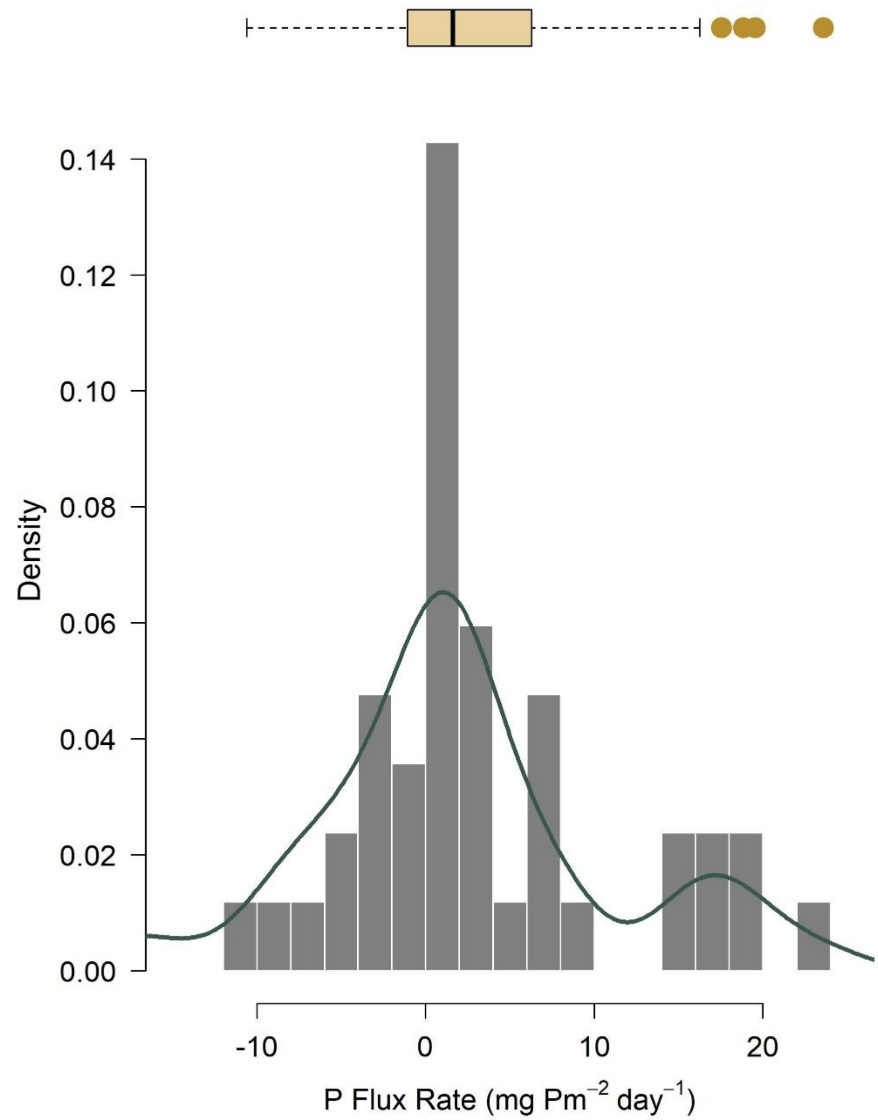

Figure S2. *Distribution of sediment P flux rates.* The histogram details measured sediment P flux rates over all sampling sites and seasons while the density curve provides a kernel density estimation. The distribution and statistical outliers are further summarized with a boxplot.

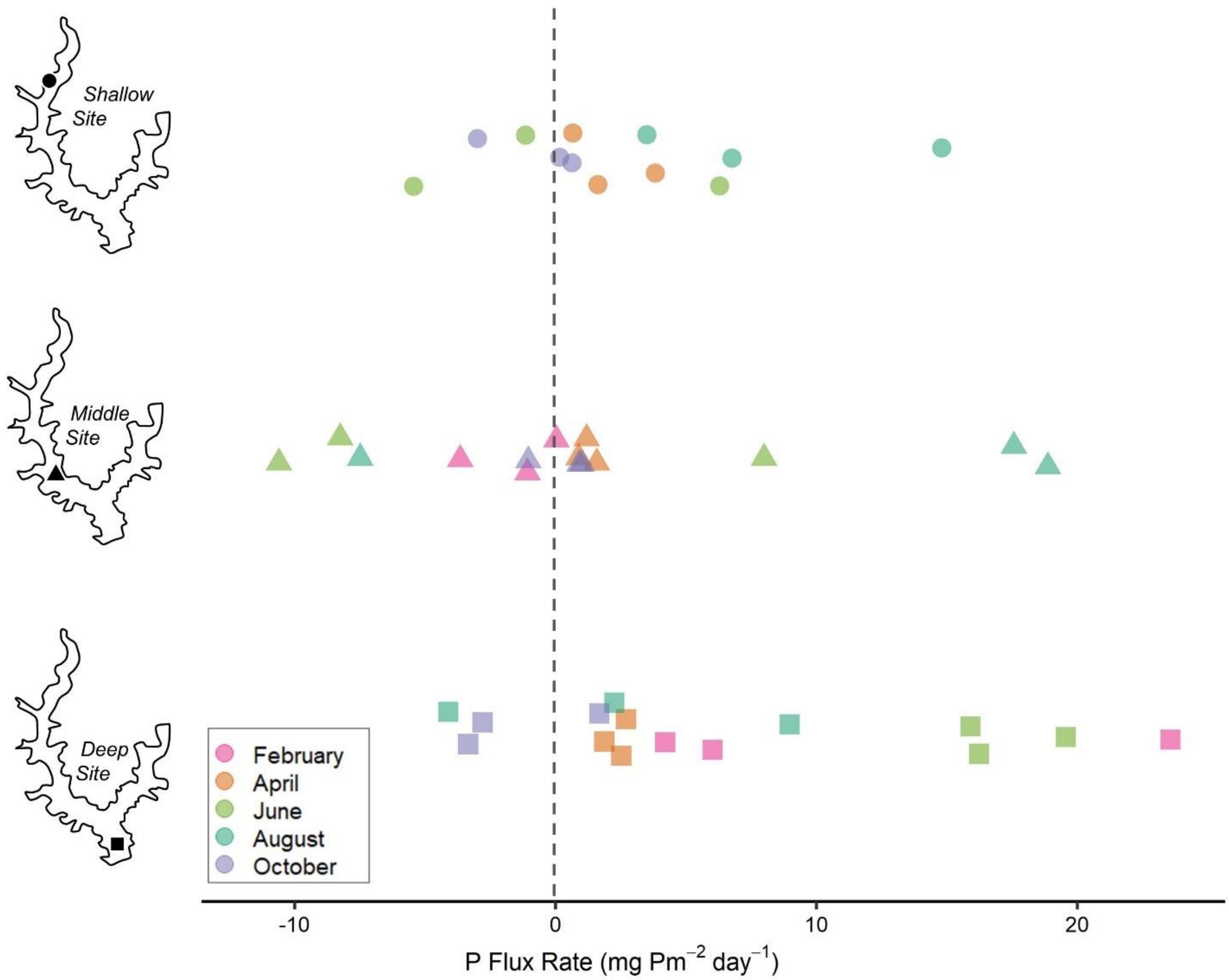

Figure S3. *Sediment P flux rates by site and sampling event, 2020.* The distribution of all measured sediment P flux rates is visualized by sampling site and month. The highest observed release rates were associated with sediments from the deep sampling site in February and June as well as August fluxes from the middle and shallow sites. The four highest rates are statistical outliers.

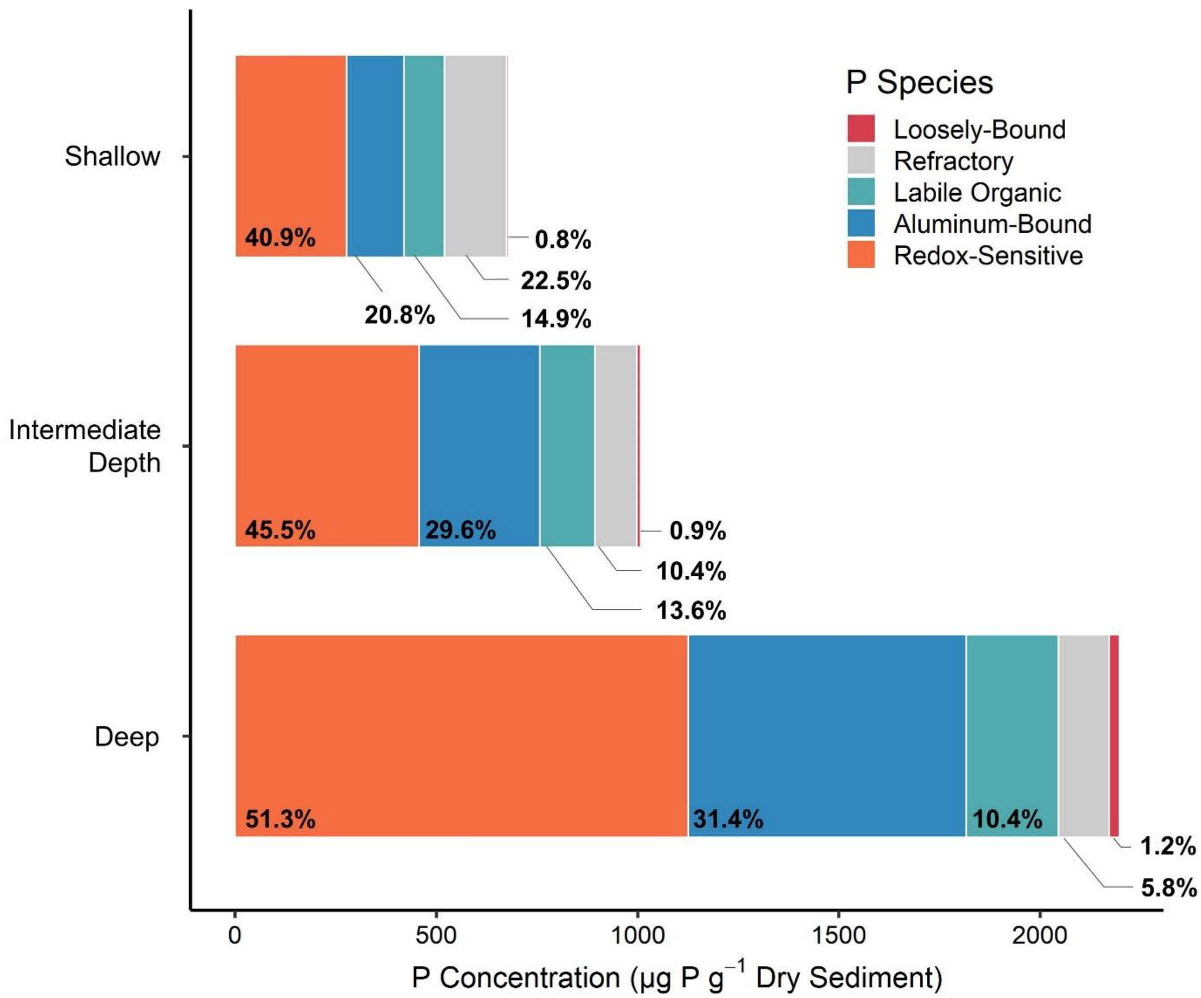

Figure S4. *Average, annual sediment P composition by sampling site.* Raw concentrations increased from the shallow to the deep site. The relative abundance of each P species as a percent of the total sediment P pool was similar among sites.

CITATIONS

Supplementary Methods Text

1. Childress CJO, Foreman WT, Conner BF, Maloney TJ. 1999. New Reporting Procedures Based on Long-Term Method Detection Levels and Some Considerations for Interpretations of Water-Quality Data Provided by the U.S. Geological Survey National Water Quality Laboratory. U.S. Geological Survey Open File Report 99-193. 24 p.
2. Crumpton WG, Isenhart TM, Mitchel PD. 1992. Nitrate and organic N analyses with second-derivative spectroscopy. Limnology and Oceanography 37(4): 907-913.
3. Håkanson L, Jansson M. 2002. Principles of lake sedimentology. Caldwell, NJ: The Blackburn Press.
4. Standard Methods for the Examination of Water and Wastewater. 1998. 20th Edition. Method 4500-N N.C.

R Packages Used for Data Cleaning and Visualizations

tidyverse (Wickham and others 2019), RColorBrewer (Neuwirth 2014), gridExtra (Auguie 2017), cowplot (Wilke 2020), ggspatial (Dunnington 2021)

1. Auguie B. 2017. gridExtra: Miscellaneous Functions for "Grid" Graphics. R package version 2.3.
2. Dunnington D. 2021. ggspatial: Spatial Data Framework for ggplot2. R package version 1.1.5.
3. Neuwirth E. 2014. RColorBrewer: ColorBrewer Palettes. R package version 1.1-2.
4. Wickham H, Averick M, Bryan J, Chang W, D'Agostino McGowan L, François R, Grolemund G, Hayes A, Henry L, Hester J, Kuhn M, Pedersen TL, Miller E, Bache SM, Müller K, Ooms J, Robinson D, Seidel DP, Spinu V, Takahashi K, Vaughan Dand, Wilke C, Woo K, Yutani H. 2019. 2019. Welcome to the tidyverse. Journal of Open Source Software 4(43): 1686.
5. Wilke CO. 2020. cowplot: Streamlined Plot Theme and Plot Annotations for 'ggplot2'. R package version 1.1.1.